ACS APPLIED MATERIALS & INTERFACES

Research Article

www.acsami.org

Effect of Copper Oxide Oxidation State on the Polymer-Based Solar Cell Buffer Layers

Hsiang-Ting Lien,[†,‡] Deniz P. Wong,[†,§] Nai-Hung Tsao,[§,∥] Ching-I Huang,[‡] Chaochin Su,[∥] Kuei-Hsien Chen,*[,†,§] and Li-Chyong Chen*[,†]

[†]Center for Condensed Matter Sciences, National Taiwan University, Taipei 10617, Taiwan, R.O.C.

[‡]Institute of Polymer Science and Engineering, National Taiwan University, Taipei 10617, Taiwan, R.O.C.

[§]Institute of Atomic and Molecular Sciences, Academia Sinica, Taipei 10617, Taiwan, R.O.C.

[∥]Institute of Organic and Polymeric Materials, National Taipei University of Technology, Taipei 10608, Taiwan, R.O.C.

Supporting Information

ABSTRACT: Transporting buffer layers are important components of polymer-based organic photovoltaic devices. In this study, we have investigated the effects of the oxidation state in copper oxide based buffer layer in conjunction to its role in device performance. We have shown that variation in the oxidation state affects the band alignment and built-in voltage of the device, therefore leading to variation in device performance. Specifically, the fully oxidized copper oxide buffer layer has a valence band position at 5.12 eV, much closer to the highest occupied molecular orbital of poly(3-hexylthiophene-2,5-diyl) (P3HT) (~5.2 eV), giving a best fill factor and efficiency at 57% and 4.06%, respectively. Lastly, we also demonstrate significant enhancement in device stability, with power conversion efficiency maintained at 75% of the original value even after 40 days, and propose a strategy for recovering the device performance based on the observed property of the oxide buffer layer.

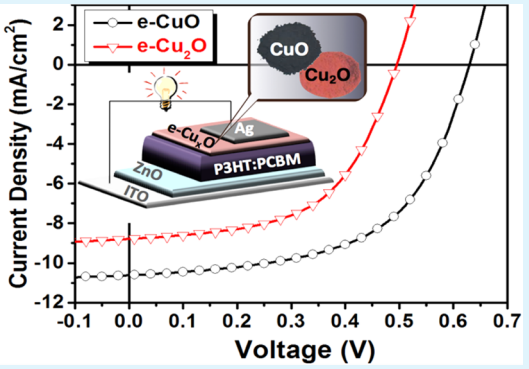

KEYWORDS: *buffer layer, copper oxide, photovoltaics, X-ray absorption*

1. INTRODUCTION

Recent developments on organic photovoltaics (OPVs) have shown steady signs of improvement and niche targeted applications. OPVs have attracted high attention due to several advantages compared to a traditional PV system such as their ease of processing, low cost, scalability to large area fabrication, and light weight.[1−5] In the last five years, the highest power conversion efficiency (PCE) that has been reported reaches to above 9−10%.[6,7] This can still be further improved by optimizing processing conditions, such as modification and/or development of effective buffer layers that act as a bridge between the electrodes and the active materials.[8,9] The buffer layers have been reported to reduce the energy loss by improving the band alignment between the active material and the electrode.[10,11] Moreover, they are also known to act as optical spacers and protection layers for the solar cell devices.[12,13] Poly(3,4-ethylenedioxythiophene):poly-(styrenesulfonate) (PEDOT:PSS) is one of the commonly used materials that acts as a hole transporting buffer layer (HTL). However, its acidic nature and instability to moisture has a negative influence on device performance and overall device stability.[14,15] On the other hand, transition metal oxides such as MoO_x,[16−18] V_2O_5,[19] NiO,[20] and CuO_x[21,22] have shown to overcome those problems and even offer better device performance. Although there are a lot of reports demonstrating the effectiveness of oxides as a buffer layer, there are still fundamental questions regarding their influence on the device properties. One of these questions is on the oxidation state of these oxides and their influence on the PCE and device stability.[23]

Transition metal oxides often consist of several known oxidation states. Studies by Lee et al. have shown that the oxidation state of the molybdenum oxide as buffer layer strongly correlates with the device efficiency.[17] Furthermore, Kim et al. also show that a different oxidation state of CuO_x influences the gap states found near the Fermi level, which was shown to be the origin of the hole transport path in their organic light emitting diode (OLED) system.[24]

In this study, we use copper oxide as a model material to demonstrate the effect of oxidation state on the buffer layer properties in relation to device performance and stability. Copper oxide (Cu_xO) has two known stable oxidation states, cupric oxide (CuO) and cuprous oxide (Cu_2O). Furthermore, Cu_xO offers several advantages as transporting buffer layer in OPV application such as being earth-abundant, nontoxic, and low cost and having good p-type conductivity (hole transport

Received: September 19, 2014
Accepted: November 18, 2014
Published: November 18, 2014

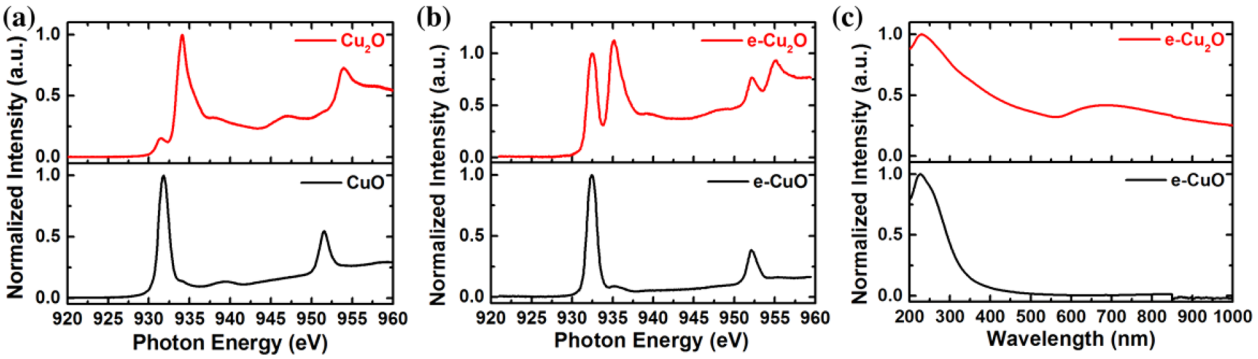

Figure 1. Cu L-edge X-ray absorption spectrum of (a) CuO and Cu_2O powders, (b) e-CuO and e-Cu_2O films, and (c) the corresponding normalized UV−visible absorption spectrum of the e-Cu_xO films.

layer).[25] Previous studies of Cu_xO as transport layer have shown that it can improve the Ohmic contact of the active material with the metal electrode and at the same time redistribute the light intensity to enhance photoabsorption.[21] However, the lack of control in the oxidation state of Cu_xO from the solution-based process makes it difficult to assess the effect of oxidation state on the ultimate device performance and stability. Similar studies have demonstrated that additional treatments of the solution-based films are required to improve their functionality for enhancing the device efficiency.[21,26,27] Therefore, to have a better understanding of the effect of oxidation state on the material, vacuum thermal evaporation was chosen as a deposition method of our transporting buffer layer. This also guarantees good film quality and interface smoothness between the active material and the transporting layer.

2. EXPERIMENTAL SECTION

2.1. Materials. Active materials in the photovoltaic devices were made from poly(3-hexylthiophene-2,5-diyl) (P3HT) purchased from Rieke metals and phenyl-C_{61}-butyric acid methyl ester ($PC_{61}BM$) (99.5%) from Solenne. Zinc acetate dehydrate (99.9%), 2-methoxyethanol (99%), and ethanolamine (99.5%) were purchased from Sigma-Aldrich to prepare the electron-transporting layers in the inverted solar cells. The materials of hole transporting layers, copper(II) oxide (99.99%) and copper(I) oxide (99.99%) powders, were purchased from Sigma-Aldrich. All of the other chemicals were used without any further purification.

2.2. Preparation of the Inverted Photovoltaic Device. Prior to usage, patterned indium tin oxide (ITO) was cleaned with detergent, deionized water, acetone, and isopropyl alcohol by ultrasonic bath for 10 min, then dried by N_2 gas and heated at 150 °C for 10 min. The preparation of ZnO sol−gel precursor solution was described elsewhere.[12,13] The solution was spin-coated on ITO at 4000 rpm for 40 s, then annealed on a hot plate for 10 min for 150 °C to form a uniform ZnO film. The formulation of the active layer contains 2% of P3HT and $PC_{61}BM$ (with weight ratio of 1:1) dissolved in chlorobenzene and stirred in a glovebox environment for 12 h before usage. The active layer was spin-coated on top of the ZnO film on ITO at 1000 rpm for 45 s under ambient atmosphere, which produced ∼150 nm thick film after annealing in the glovebox for 10 min at 150 °C. The different hole transport layers were deposited via thermal-evaporated oxide film or spin-coated PEDOT:PSS on the active layer before deposition of the top metal contact. The thermal-evaporated copper oxide (e-Cu_xO) films were obtained from direct evaporation of CuO (denoted as e-CuO) or Cu_2O (denoted as e-Cu_2O) powder under vacuum around 10^{-6} Torr. The Ag film, as metal contact electrode, was thermally deposited to a thickness of 100 nm in vacuum with a backpressure around 10^{-6} Torr. The active area of the photovoltaic device was 0.04 cm^2, which was determined by the shadow mask during electrode deposition.

2.3. Device Measurement and Thin Film Characterization. The current density versus voltage (J−V) characteristics of devices were measured in ambient atmosphere with and without light illumination using simulated solar light (AM 1.5 G, 100 mW/cm^2). All of the electrical data was recorded by a Keithley 2400 sourcemeter. The incident photon-to-current efficiency (IPCE) spectra were conducted using a 150 W xenon lamp source with a monochromator and light spot size of 1 mm × 1 mm, and the signal was obtained via a lock-in amplifier.

For the characterization of the oxide films, the tapping-mode atomic force microscopy (AFM) images were obtained by a JPK NanoWizard II. This is to observe the surface morphologies of oxide films deposited on top of the active material surface. Composition of e-Cu_xO films was determined by L-edge X-ray absorption spectroscopy, which was conducted in beamline 20A1 at National Synchrotron Radiation Research Center (NSRRC) in Hsin-Chu. X-ray diffraction patterns were obtained using Bruker D8 Advanced diffractometer with a Cu Kα source (λ = 1.5405 Å). UV−vis absorption spectrometry was performed using a JASCO 670 spectrometer.

3. RESULTS AND DISCUSSION

3.1. Characterization of Cu_xO Films. Morphological and optical studies were conducted on the evaporated oxide films.

Scheme 1. Band Energy Configuration of OPV Using Various Buffer Layers

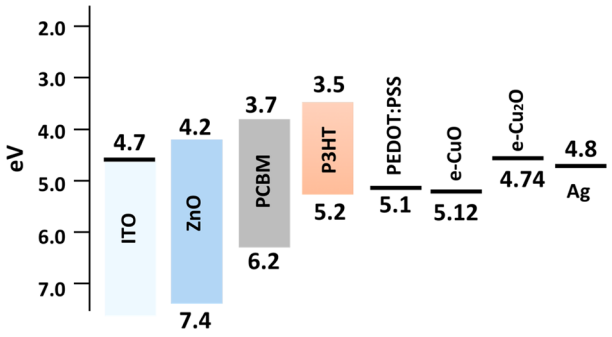

X-ray diffraction patterns indicated that both films were similarly amorphous (Figure S1, Supporting Information). Furthermore, atomic force micrographs showed that the surfaces of both films were smooth with root-mean-square value of roughness around 700 pm (Figure S2, Supporting Information). The level of smoothness of the films ensures good contact between the anode and the photoactive layer where hole collection is being facilitated.

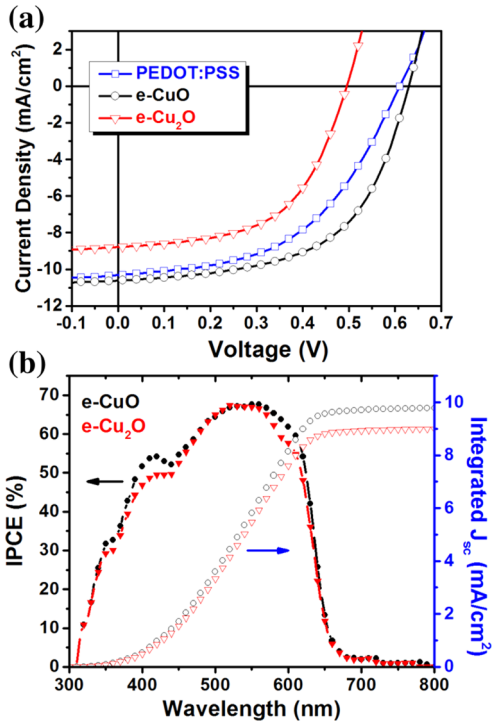

Figure 2. (a) Current density vs voltage ($J-V$) curves and (b) IPCE spectra and their integrated current density of OPV devices using different hole transporting buffer layers.

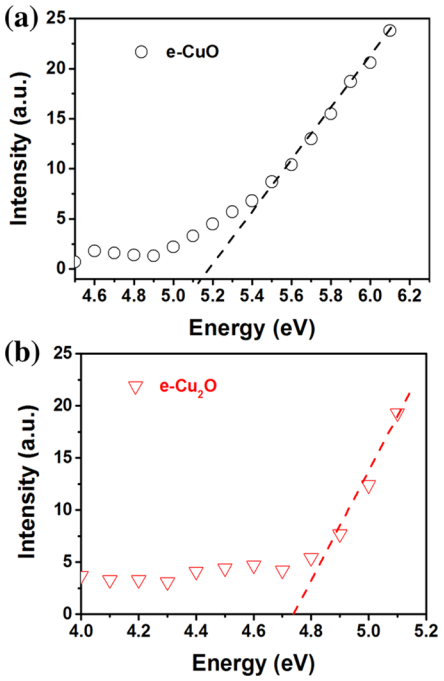

Figure 3. Photoelectron spectra in air of (a) e-CuO film and (b) e-Cu_2O film on top of the bulk heterojunction (BHJ) layer.

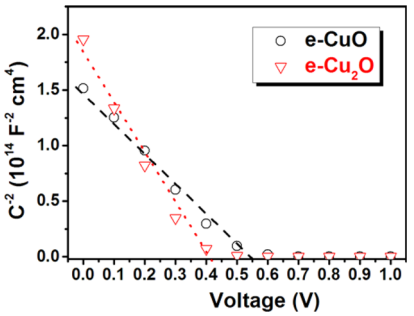

Figure 4. Mott−Schottky plot of the OPVs using different oxide buffer layers.

Because no significant differences were observed from the aforementioned characterization tools, an X-ray absorption spectroscopic (XAS) study was employed to distinguish both groups of films. As a reference, the same technique has been applied to both CuO and Cu_2O powder samples, which indeed showed two characteristically different spectra (Figure 1a) for Cu L-edge, where the core electron was excited from the $2p_{1/2}$ or $2p_{3/2}$ to the unoccupied 3d state. Two prominent features corresponding to L_{III} (930−940 eV) and L_{II} edge (950−960 eV) were observed. A literature survey indicates that pure CuO shows peaks around 932 eV for L_{III} edge and 952 eV for L_{II} edge, whereas pure Cu_2O shows peaks around 935 eV for L_{III} edge and 955 eV for L_{II} edge.[28] From Figure 1b, the e-CuO film has shown peaks similar to that with pure CuO while e-Cu_2O has shown peaks from both CuO and Cu_2O, indicating single-phase and mixed oxides were formed in the former and latter processes, respectively.

In addition to XAS measurements, visible absorption spectra were also obtained for both films. As shown in Figure 1c, the normalized absorption spectrum from e-CuO film clearly indicates a single absorption edge, which translates to an optical band gap of 1.76 eV. In contrast, e-Cu_2O film has shown two absorption edges, which translates to an optical band gap of 1.50 eV and an additional one at 2.58 eV. The former band gap value can be attributed to the CuO phase and the latter to the Cu_2O phase.[29]

3.2. Device Performance. Inverse structure (Scheme 1) organic solar cell was fabricated to gauge the potential of the copper oxide films as a hole transporting buffer layer. The current density versus voltage ($J-V$) curves (Figure 2a) show that the e-CuO containing device offers a better device performance compared to PEDOT:PSS and e-Cu_2O containing devices. From Table 1, the different solar cell metrics indicated that the e-CuO containing device performs better than its traditional PEDOT:PSS based counterpart; especially the increase in its fill factor is most significant. One of the

Table 1. Solar Cell Device Metrics of OPVs Using Different Hole Transporting Buffer Layers under AM 1.5 G and 100 mW/cm^2 Light Intensity

				efficiency		
device	V_{oc} (V)	J_{sc} (mA/cm^2)	FF (%)	avg	best	Rs (Ω)
PEDOT:PSS	0.61 ± 0.0	10.27 ± 0.06	49.9 ± 0.2	3.12 ± 0.05	3.29	322 ± 23
e-CuO	0.63 ± 0.1	10.98 ± 0.32	57.1 ± 2.4	3.91 ± 0.10	4.06	122 ± 10
e-Cu_2O	0.50 ± 0.1	8.96 ± 0.16	55.8 ± 0.5	2.41 ± 0.06	2.52	142 ± 12

dx.doi.org/10.1021/am5064469 | ACS Appl. Mater. Interfaces 2014, 6, 22445−22450

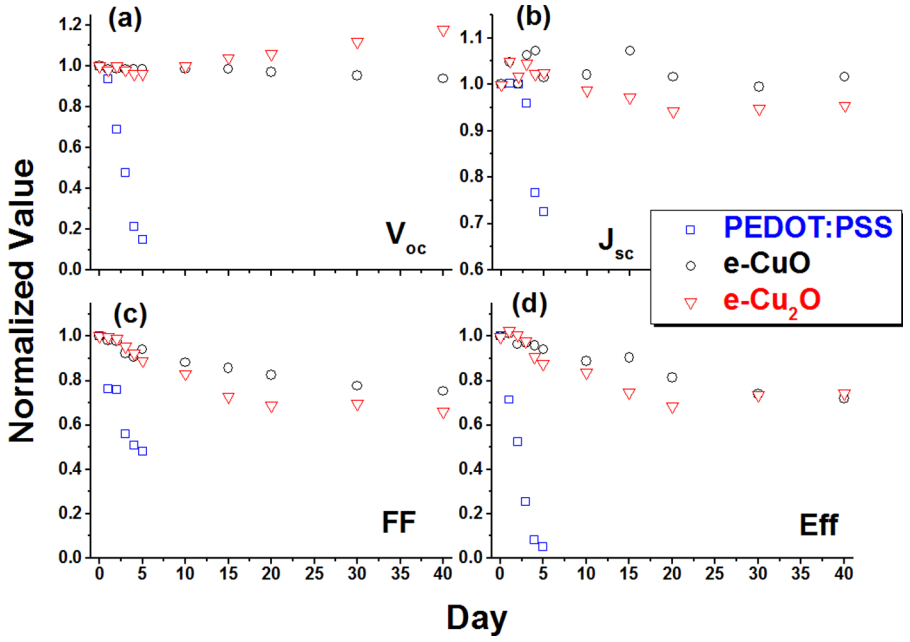

Figure 5. Solar cell device metrics ((a) V_{oc}, (b) J_{sc}, (c) fill factor (FF), and (d) efficiency) measured in a span of 40 days.

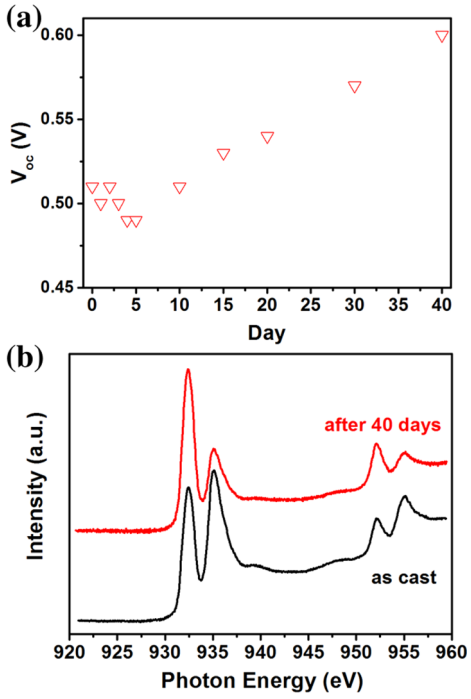

Figure 6. (a) Time-dependent V_{oc} of OPV device using e-Cu_2O film and the corresponding (b) Cu L edge XAS of the as-cast film and the one after 40 days.

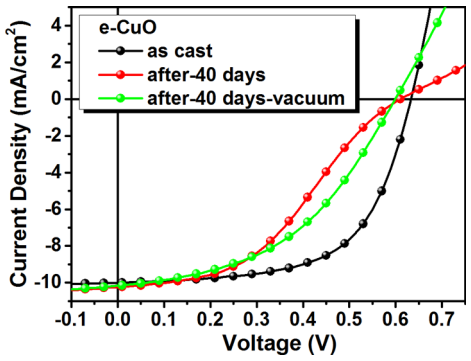

Figure 7. *J*–*V* curves of e-CuO containing devices under different conditions.

reasons—smoothness of the e-CuO films—creates better interface with the metal contact, resulting in an enhanced fill factor with the decrease in series resistance. In contrast, the e-Cu_2O containing device has shown the lowest efficiency among the three, which is mainly due to the much reduced short circuit current and lower open circuit voltage, while maintaining a fill factor similar to that of its e-CuO counterpart. The difference in photocurrent can be explained through the IPCE spectra. The IPCE spectra (Figure 2b) of the e-Cu_xO containing devices show a strong resemblance to the absorption spectra of the active materials with maximum value at the range of 450–550 nm. Notice that the e-CuO device had the highest IPCE value with larger responses than the e-Cu_2O device in the region of 400–450 nm and 600–650 nm. The integration of the IPCE spectra with AM 1.5 solar spectrum (Figure 2b) gives a current density of each device that is in good agreement with the one measured using the solar simulator.

Meanwhile, the differences in the open circuit voltage can be explained by the mismatch of band position of e-Cu_2O films with the energy levels of the active materials and the current collector (anode). As revealed from the photoelectron spectra (Figure 3), the valence band positions of e-Cu_2O and e-CuO films are at 4.74 and 5.12 eV, respectively. Energy-level alignment illustrated in Scheme 1 shows that the valence band of e-CuO film is closer to the highest occupied molecular orbital (HOMO) of P3HT (~5.2 eV). This implies that holes can easily transport to the Ag anode without any significant losses, therefore leading to better device performance. In contrast, the valence band of e-Cu_2O film is slightly lower than the band edge of the Ag anode and far from the HOMO of the active material. Therefore, the transport pathway of the carriers is impeded from the active material to the current collector,

dx.doi.org/10.1021/am5064469 | ACS Appl. Mater. Interfaces 2014, 6, 22445–22450

resulting in significant losses due to the larger barrier to overcome before passing through.

To further understand the role of the oxide in the organic solar cell, capacitance−voltage ($C-V$) measurements were performed. Using Mott−Schottky analysis (Figure 4), the built-in voltage of the devices can be evaluated, by finding the x-intercept of the linear regime from the Mott−Schottky plot. The values obtained are 0.55 V for e-CuO and 0.42 V for e-Cu_2O. The difference between the two values corresponds also to the difference between the V_{oc} of both devices containing the respective oxide material. The upward shift of the built-in voltage of ∼130 mV for the e-CuO containing device indicates a more efficient separation of the photogenerated carriers, which is reflected in a higher photo current density. In addition, higher built-in potential also indicates a larger depletion region at the interface, thus suppressing exciton recombination.[30]

3.3. Lifetime Study of Oxide Containing Devices. In addition to the benefits in electrical pathways, the transporting buffer layer is also reported to improve stability of the solar cell device. By monitoring the efficiency of the unsealed device and the corresponding solar cell metrics over the span of >1000 h (>40 days), we have observed that the oxide containing devices show superior stability improvement over the standard PEDOT:PSS containing device. Figure 5 shows the degradation trend of the devices by plotting the different solar cell metrics as a function of time elapsed.

After 5 days of testing, we observed that the PEDOT:PSS device was unstable. The corresponding V_{oc} dropped to 15% and the J_{sc} dropped to ∼70%, while FF dropped to 50% of the original. This corresponds to a dramatic decrease of the PCE to ∼5% of the original. Previous studies have indicated that the stability issue of the PEDOT:PSS containing device is due to the shift in work function of PEDOT:PSS, whose property is affected by the water content.[10]

In contrast, the lifetime study for the e-Cu_xO containing devices indicates substantially improved stability, as their PCE only dropped to 75% of the original value even after 40 days of testing. However, the trends of the solar cell metrics for the devices using the two different types of buffer layers showed some differences. The e-CuO containing device has maintained its V_{oc} and J_{sc} values in the span of >40 days; however, its FF value dropped to 75% of the original, which corresponds to the drop in the PCE value. On the other hand, the e-Cu_2O containing device follows a peculiar trend of decreasing in the PCE value to lower than its e-CuO counterpart in 20 days and increasing back to about the same level after 40 days. This is due to the increase in the V_{oc} value from 0.5 to 0.6 V (Figure 6a). The improvement can be attributed to the transformation of the Cu_2O phase present in e-Cu_2O to the CuO phase. Figure 6b shows the L-edge XAS spectra of e-CuO_x film as cast and after 40 days. As mentioned previously, the significant reduction of peak intensity at 935 and 955 eV indicates the decrease of the Cu_2O phase, and the corresponding increase in the intensity at 932 and 952 eV indicates the increase in the CuO phase.

For the oxide containing devices, the decrease of the PCE can be attributed to the decrease in FF. The $J-V$ curve (Figure 7) of the e-CuO containing device after 40 days show a typical S-shape curve, which indicates incorrect dipole formation at the interface causing accumulation of charges, thus impeding the transport path way.[31] Because diffusion of water into the oxide barrier is more difficult than in the PEDOT:PSS, we can maintain the band position of the oxide in the device structure unlike in the latter material. The stable V_{oc} and J_{sc} values in the oxide containing device indicate an intact active material without significant degradation. This suggests that accumulation of the water and/or oxygen molecules occurs at the interface of the oxide layer and the metal electrode. If this is the case, removing the accumulation of unwanted molecules at the interface can revert back the decrease in FF. Figure 7 shows that, by putting the device in vacuum (10^{-2} Torr) for 2 days, an increase in FF is observed. This demonstrates that we can further develop our process by improving the stability of the device.

4. CONCLUSION

In conclusion, we have demonstrated the use of Cu_xO as an effective hole transporting buffer layer by improving the device performance as well as its stability. A PCE of 4.06% was achieved using a P3HT:PC_{61}BM based solar cell with device degradation of only 25% after 40 days. Furthermore, from our various analyses, we have also shown that it is important for the oxide material to have a correct band alignment with the active material and the metal electrode. In addition, a fully oxidized state of the material is also desirable to ensure its stability and at the same time maintain the corresponding device performance.

■ ASSOCIATED CONTENT

Ⓢ Supporting Information

XRD data and AFM image of e-Cu_xO film. This material is available free of charge via the Internet at http://pubs.acs.org.

■ AUTHOR INFORMATION

Corresponding Authors

*E-mail: chenkh@pub.iams.sinica.edu.tw.

*E-mail: chenlc@ntu.edu.tw.

Notes

The authors declare no competing financial interest.

■ ACKNOWLEDGMENTS

This research was financially supported by the Ministry of Education, Ministry of Science and Technology, Academia Sinica (Taiwan). Technical support was provided by the Core Facilities for Nano Science and Technology, National Synchrotron Radiation Research Center, Academia Sinica, and National Taiwan University.

■ REFERENCES

(1) Yu, G.; Gao, J.; Hummelen, J. C.; Wudl, F.; Heeger, A. J. Polymer Photovoltaic Cells: Enhanced Efficiencies via a Network of Internal Donor-Acceptor Heterojunctions. *Science* **1995**, *270*, 1789−1791.

(2) Li, G.; Shrotriya, V.; Huang, J.; Yao, Y.; Moriarty, T.; Emery, K.; Yang, Y. High-Efficiency Solution Processable Polymer Photovoltaic Cells by Self-Organization of Polymer Blends. *Nat. Mater.* **2005**, *4*, 864−868.

(3) Servaites, J. D.; Ratner, M. A.; Marks, T. J. Organic Solar Cells: A New Look at Traditional Models. *Energy Environ. Sci.* **2011**, *4*, 4410−4422.

(4) Li, G.; Zhu, R.; Yang, Y. Polymer Solar Cells. *Nat. Photonics* **2012**, *6*, 153−161.

(5) Heeger, A. J. 25th Anniversary Article: Bulk Heterojunction Solar Cells: Understanding the Mechanism of Operation. *Adv. Mater.* **2014**, *26*, 10−28.

(6) He, Z.; Zhong, C.; Su, S.; Xu, M.; Wu, H.; Cao, Y. Enhanced Power-Conversion Efficiency in Polymer Solar Cells Using an Inverted Device Structure. *Nat. Photonics* **2012**, *6*, 591−595.

(7) You, J.; Dou, L.; Yoshimura, K.; Kato, T.; Ohya, K.; Moriarty, T.; Emery, K.; Chen, C.-C.; Gao, J.; Li, G.; Yang, Y. A Polymer Tandem Solar Cell with 10.6% Power Conversion Efficiency. *Nat. Commun.* **2013**, *4*, 1466.
(8) Chang, C. C.; Lin, C. F.; Chiou, J. M.; Ho, T. H.; Tai, Y.; Lee, J. H.; Chen, Y. F.; Wang, J. K.; Chen, L. C.; Chen, K. H. Effects of Cathode Buffer Layers on the Efficiency of Bulk-Heterojunction Solar Cells. *Appl. Phys. Lett.* **2010**, *96*, 263506.
(9) Han, H. C.; Tseng, C. A.; Du, C. Y.; Ganguly, A.; Chong, C. W.; Wang, S. B.; Lin, C. F.; Chang, S. H.; Su, C. C.; Lee, J. H.; Chen, K. H.; Chen, L. C. Enhancing Efficiency with Fluorinated Interlayers in Small Molecule Organic Solar Cells. *J. Mater. Chem.* **2012**, *22*, 22899–22905.
(10) Po, R.; Carbonera, C.; Bernardi, A.; Camaioni, N. The Role of Buffer Layers in Polymer Solar Cells. *Energy Environ. Sci.* **2011**, *4*, 285–310.
(11) Kumar, A.; Rosen, N.; Devine, R.; Yang, Y. Interface Design to Improve Stability of Polymer Solar Cells for Potential Space Applications. *Energy Environ. Sci.* **2011**, *4*, 4917–4920.
(12) Kyaw, A. K. K.; Wang, D. H.; Wynands, D.; Zhang, J.; Nguyen, T. Q.; Bazan, G. C.; Heeger, A. J. Improved Light Harvesting and Improved Efficiency by Insertion of an Optical Spacer (ZnO) in Solution-Processed Small-Molecule Solar Cells. *Nano Lett.* **2013**, *13*, 3796–3801.
(13) Sun, Y.; Seo, J. H.; Takacs, C. J.; Seifter, J.; Heeger, A. J. Inverted Polymer Solar Cells Integrated with a Low-Temperature-Annealed Sol-Gel-Derived ZnO Film as an Electron Transport Layer. *Adv. Mater.* **2011**, *23*, 1679–1683.
(14) Girtan, M.; Rusu, M. Role of ITO and PEDOT:PSS in Stability/Degradation of Polymer:Fullerene Bulk Heterojunctions Solar Cells. *Sol. Energy Mater. Sol. Cells* **2010**, *94*, 446–450.
(15) Xia, Y.; Zhang, H.; Ouyang, J. Highly Conductive PEDOT:PSS Films Prepared through a Treatment with Zwitterions and Their Application in Polymer Photovoltaic Cells. *J. Mater. Chem.* **2010**, *20*, 9740–9747.
(16) Shrotriya, V.; Li, G.; Yao, Y.; Chu, C. W.; Yang, Y. Transition Metal Oxides as the Buffer Layer for Polymer Photovoltaic Cells. *Appl. Phys. Lett.* **2006**, *88*, 073508.
(17) Lee, Y. J.; Yi, J.; Gao, G. F.; Koerner, H.; Park, K.; Wang, J.; Luo, K.; Vaia, R. A.; Hsu, J. W. P. Low-Temperature Solution-Processed Molybdenum Oxide Nanoparticle Hole Transport Layers for Organic Photovoltaic Devices. *Adv. Energy Mater.* **2012**, *2*, 1193–1197.
(18) Murase, S.; Yang, Y. Solution Processed MoO_3 Interfacial Layer for Organic Photovoltaics Prepared by a Facile Synthesis Method. *Adv. Mater.* **2012**, *24*, 2459–2462.
(19) Baeg, K. J.; Bae, G. T.; Noh, Y. Y. Efficient Charge Injection in p-Type Polymer Field-Effect Transistors with Low-Cost Molybdenum Electrodes through V_2O_5 Interlayer. *ACS Appl. Mater. Interfaces* **2013**, *5*, 5804–5810.
(20) Steirer, K. X.; Chesin, J. P.; Widjonarko, N. E.; Berry, J. J.; Miedaner, A.; Ginley, D. S.; Olson, D. C. Solution Deposited NiO Thin-Films as Hole Transport Layers in Organic Photovoltaics. *Org. Electron.* **2010**, *11*, 1414–1418.
(21) Lin, M. Y.; Lee, C. Y.; Shiu, S. C.; Wang, I. J.; Sun, J. Y.; Wu, W. H.; Lin, Y. H.; Huang, J. S.; Lin, C. F. Sol–Gel Processed CuO_x Thin Film as an Anode Interlayer for Inverted Polymer Solar Cells. *Org. Electron.* **2010**, *11*, 1828–1834.
(22) Xu, Q.; Wang, F.; Tan, Z. a.; Li, L.; Li, S.; Hou, X.; Sun, G.; Tu, X.; Hou, J.; Li, Y. High-Performance Polymer Solar Cells with Solution-Processed and Environmentally Friendly CuO_x Anode Buffer Layer. *ACS Appl. Mater. Interfaces* **2013**, *5*, 10658–10664.
(23) Lee, J. S.; Jang, I. H.; Park, N. G. Effects of Oxidation State and Crystallinity of Tungsten Oxide Interlayer on Photovoltaic Property in Bulk Hetero-Junction Solar Cell. *J. Phys. Chem. C* **2012**, *116*, 13480–13487.
(24) Kim, S.; Hong, K.; Kim, K.; Lee, I.; Lee, J. L. Phase-Controllable Copper Oxides for an Efficient Anode Interfacial Layer in Organic Light-Emitting Diodes. *J. Mater. Chem.* **2012**, *22*, 2039–2044.
(25) Lavareda, G.; Carvalho, C. N. d.; Ferraria, A. M.; Rego, A. M. B. d.; Amaral, A. p-Type CuO_x Thin Films by RF-Plasma Enhanced Reactive Thermal Evaporation: Influence of RF-Power Density. *J. Nanosci. Nanotechnol.* **2012**, *12*, 6754–6757.
(26) Frey, G. L.; Reynolds, K. J.; Friend, R. H.; Cohen, H.; Feldman, Y. Solution-Processed Anodes from Layer-Structure Materials for High-Efficiency Polymer Light-Emitting Diodes. *J. Am. Chem. Soc.* **2003**, *125*, 5998–6007.
(27) Kato, S.; Ishikawa, R.; Kubo, Y.; Shirai, H.; Ueno, K. Efficient Organic Photovoltaic Cells Using Hole-Transporting MoO_3 Buffer Layers Converted from Solution-Processed MoS_2 Films. *Jpn. J. Appl. Phys.* **2011**, *50*, 071604.
(28) Chen, C. L.; Rao, S. M.; Wang, K. J.; Hsu, F. C.; Lee, Y. C.; Dong, C. L.; Chan, T. S.; Lee, J. F.; Ling, M. C.; Liu, H. L.; Wu, M. K. Investigation of the Unoccupied States in Sr_2YRuO_6 Single Crystals Doped with Cu. *New J. Phys.* **2009**, *11*, 073024.
(29) Balamurugan, B.; Mehta, B. R. Optical and Structural Properties of Nanocrystalline Copper Oxide Thin Films Prepared by Activated Reactive Evaporation. *Thin Solid Films* **2001**, *396*, 90–96.
(30) Laban, W. A.; Etgar, L. Depleted Hole Conductor-Free Lead Halide Iodide Heterojunction Solar Cells. *Energy Environ. Sci.* **2013**, *6*, 3249–3253.
(31) Kumar, A.; Sista, S.; Yang, Y. Dipole Induced Anomalous S-Shape I-V Curves in Polymer Solar Cells. *J. Appl. Phys.* **2009**, *105*, 094512.